Int. J. High Technology Ceramics **3** (1987) 199–230

High Temperature Creep and Slow Crack Growth Properties of HPSN as an Example of Ceramics Containing a Glassy Phase

D. Bethge*

Kernforschungszentrum Karlsruhe, Postfach 3640, 7500 Karlsruhe, FRG

SUMMARY

The high temperature creep kinetics and the slow propagation of cracks in hot-pressed silicon nitride with a glassy phase were investigated. In addition, creep tests under constant load (4-point-bending), compliance measurements and stress relaxation experiments were carried out. Specimens with trapezoidal cross sections were used to determine the ratio of the creep rates in tension and compression. A two phase model, based on the compliance measurements, describes well the kinetics of primary creep.

A consideration of the strength criterion for slow crack growth can be neglected for materials undergoing viscous flow or creep. A crack propagates, whenever the free energy of the sample is thereby lowered. Assuming that the voids nucleated in the near crack stress field and in the whole (creeping) specimen contribute to crack propagation, theory and experiments are in agreement.

LIST OF NOTATIONS

A, A_t, A_c	Creep parameter (t: tension, c: compression)
D	Increment $d\dot{\varepsilon}/dy$
E	Young's modulus

* Present address: Nixdorf Computer AG, Postfach 2160, 4790 Paderborn, FRG.

Int. J. High Technology Ceramics 0267-3762/87/$03·50

E'	$E/(1-\nu)$
G	Energy releasing rate
K_I	Stress intensity factor
K_{IC}	Critical stress intensity factor
M	Bending moment
N	Exponent
$\tilde{N}$	Void or microcrack density
P	Load
$\tilde{P}$	Constant factor (with index)
T	Temperature
U	Elastic energy
V, V_ρ, V_ε	Porosity (ρ: porosity nucleated in the near crack tip stress field, ε: creep porosity)
W	Work done by the external forces
W^*	Energy term for crack propagation
a	Crack length
$\dot{a}$	Crack velocity
b	Specimen width
c	Exponent
f, f_m	Displacement (m: middle deflection)
h, h_t, h_c	Specimen height (t: tension zone, c: compression zone)
i	Number of grain contacts per unit volume
k, m, n, q	Exponent
r	Radius
t	Time
t^*	Fictitious time
t_r	Rupture time
y, η	Coordinate
$\alpha_1, \alpha_2, \alpha_3$	Material and geometry factors
β	Constant factor (with index)
γ	Surface energy
ε	Strain
ε^*	ε of the outer bend fibre, calculated like in the elastic case
$\dot{\varepsilon}$	Creep rate
ν	Poisson's ratio
ρ	Damage zone
σ	Stress
σ^*	σ of the outer bend fibre, calculated like in the elastic case
σ_∞	Outer tensile stress in the bend specimen for $t \to \infty$
σ_e	Effective stress
σ_0	Stress for $t = 0$

1 INTRODUCTION

A study was made of the kinetics of creep and slow crack growth at high temperatures in ceramic materials containing a glassy boundary phase, i.e. HPSN. Engine designers intend to use ceramics for components exposed to temperatures above the softening level of metals. The plastic or creep deformation that occurs at these temperatures is more pronounced under tension than under compression, as has been reported earlier;[1] but what about the temperature dependence of this effect? Furthermore, the elastic properties of the specimen as a function of creep deformation and temperature were measured and are discussed. It will be shown that primary creep can be described by a mechanical two-phase model. It follows from this statement that the mechanism governing creep should change when stationary conditions are reached. The analysis of stress relaxation at constant strain is performed to complete the creep investigations.

How far do creep parameters control the slow crack growth in a creep solid? An answer to this question might be found by considering the energy-criterion for crack propagation and by suggesting that creep porosity contributes to crack propagation. This will be discussed in Section 5.

2 MATERIALS AND TEST FEATURES

The materials tested are hot pressed silicon nitride (HPSN) containing either MgO or Y_2O_3 as additives*: HPNS(Mg) and HPSN(Y).† After hot pressing, the additives form a residual, glassy boundary phase. The softening temperature of this intergranular glass is much lower than the decomposition temperature of the covalent-bonded Si_3N_4 (between 1100–1400°C, depending on glass composition compared with 1900°C at 1 bar).

For experiments (usually performed in air atmosphere) four point bend-tests were used. Outer and inner span widths of the loading apparatus were 40 and 20 mm respectively. The size of the specimens was 3·5 × 4·5 × 45 mm. A preliminary study on creep and creep failure of HPSN(Mg) with experimental details was published by G. Grathwohl.[2]

The stress distribution in the bending beam changes during the creep test because of the non-linearity between creep velocity and stress, and the different creep rates depending on whether tensile or compressive stresses are applied. Simultaneously the neutral axis shifts into the compression zone

* Commercial specifications: NH 206 and NH 209, Annawerk GmbH Rödental, FRG.
† HPSN(Y^1) has a slightly different chemical composition than HPSN(Y), (see Table 1).

TABLE 1
Chemical Composition of the Investigated Materials in Weight % (nd = not determined)

	HPSN(Mg)	*HPSN(Y)*	*HPSN(Y¹)*
Mg	2·0	0·01	0·02
Y	nd	7·8	4·6
Al	0·4	0·2	0·1
Fe	1·4	1·3	1·8

of the bend specimen. The outer tensile stress, controlling the stress intensity of surface cracks, decreases from σ^* ($=6\mathrm{M\,b^{-1}\,h^{-2}}$) to σ_∞ (Fig. 1). To describe this in dependence of time, we imagine the bend specimen composed of several fibres laying on top of each other. Each of these fibres may deform as a Maxwell spring–dashpot model. Considering the hypothesis of Bernoulli, the creep rate $\dot{\varepsilon}$ of a fibre in distance y from the specimen middle is:

$$\dot{\varepsilon}(t,y)=\frac{\dot{\sigma}}{E}+A|\sigma|^n=Dy+\dot{\varepsilon}(y=0),\qquad A=\begin{cases}A_t,\sigma>0\\-A_c,\sigma<0\end{cases}\tag{1}$$

where E is the Young's modulus and n the stress exponent of creep.

Usually for tension the dashpot or creep parameter A is greater than for compression: $A_t > A_c \times D$ is related to the middle deflection rate $\dot{f}_m$ of the specimen:

$$D=\frac{\mathrm{d}\dot{\varepsilon}}{\mathrm{d}y}=\frac{2\dot{\varepsilon}^*}{h}=\frac{2}{h}\left(0{\cdot}272\frac{4h}{l_p^2}\dot{f}_m\right)\tag{2}$$

where l_p = inner span width of loading fixture.

D and $\dot{\varepsilon}(y=0)$ depend on the actual stress distribution $\sigma(t,y)$ in the

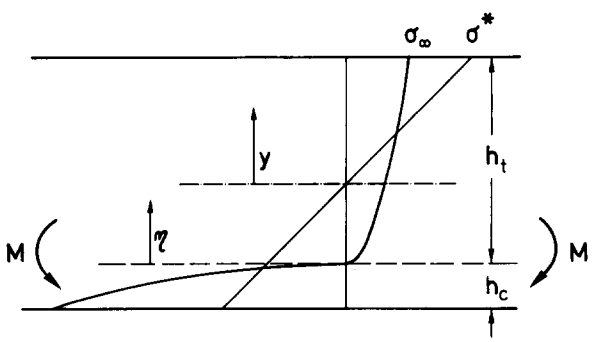

Fig. 1. Stress redistribution in the bending specimen.

specimen. In a first approximation, they can be regarded as constant and one obtains:

$$n = 1 \qquad \frac{\sigma(h/2)}{\sigma^*} = \left(1 - \frac{\sigma_\infty}{\sigma^*}\right)\exp(-A_t E t) + \frac{\sigma_\infty}{\sigma^*} \tag{3a}$$

$$n \neq 1 \qquad \frac{\sigma(h/2)}{\sigma^*} = \left\{(n-1)\sigma^{*n-1}A_t E t + \left(1 - \frac{\sigma_\infty}{\sigma^*}\right)^{1-n}\right\}^{1/(1-n)} + \frac{\sigma_\infty}{\sigma^*} \tag{3b}$$

$$\frac{\sigma_\infty}{\sigma^*} = \frac{2n+1}{6n}\left\{1 + \left(\frac{A_t}{A_c}\right)^{-1/(n+1)}\right\} \tag{4}$$

A more detailed analysis is given in reference 3.

The ratio σ_∞/σ^* can be proved by testing two bend specimen of different height with the same deflection rate ($\dot{f}_{m1} = \dot{f}_{m2} \sim d\dot{\varepsilon}/dy$, see Fig. 2). The

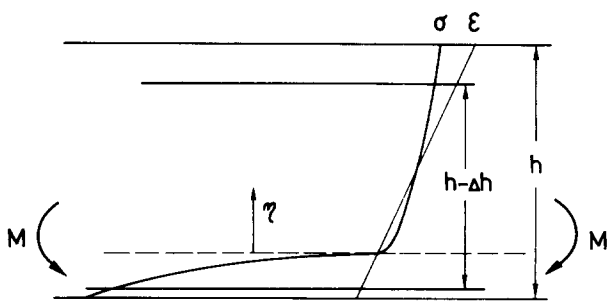

Fig. 2. Two specimens of different height ($\dot{f}_{m1} = \dot{f}_{m2} \sim d\dot{\varepsilon}/d\eta$).

bending moments are measured when stationary conditions are reached. In the small specimen the bending moment is smaller by ΔM. We find:

$$\frac{\sigma_\infty}{\sigma^*} = \frac{\Delta M h^2\left\{1 + \left(\frac{A_t}{A_c}\right)^{-1/(n+1)}\right\}}{6M\,\Delta h\left(h - \frac{\Delta h}{2}\right)} \tag{5}$$

For HPSN(Mg), 1200°C, $\dot{f}_m = 2{\cdot}1 \times 10^{-2}\,\mathrm{mm\,h^{-1}}$, for instance, we get from eqn 5: $\sigma_\infty/\sigma^* = 0{\cdot}532$. This value corresponds well with the theoretical one of eqn 4: 0·514. In Section 3 it will be shown how n and A_t/A_c are determined.

3 EXPERIMENTAL RESULTS

3.1 Primary and secondary results

The decrease of the creep rate during the primary creep range can be described mathematically by (Fig. 3):

$$\dot{\varepsilon}^* = A_1^* \sigma^{*n_1} t^c \tag{6}$$

where $\dot{\varepsilon}^*$ is calculated as for the elastic case, eqn 2.

At high temperature the value of c is $-0{\cdot}5$, it decreases to $c = -1$ with decreasing temperature (Figs 4 and 5). This temperature dependence of c is also demonstrated for other two phase ceramics.[4]

As can be seen from Figs 3 and 4, secondary or stationary creep rates are measured at 1200°C for HPSN(Mg) and at 1300°C or higher for HPSN(Y). Stationary creep usually is described through the Norton Law:

$$\dot{\varepsilon}^* = A^* \sigma^{*n} \tag{7}$$

The stress exponent n is evaluated from the creep rates which are determined at different loads.

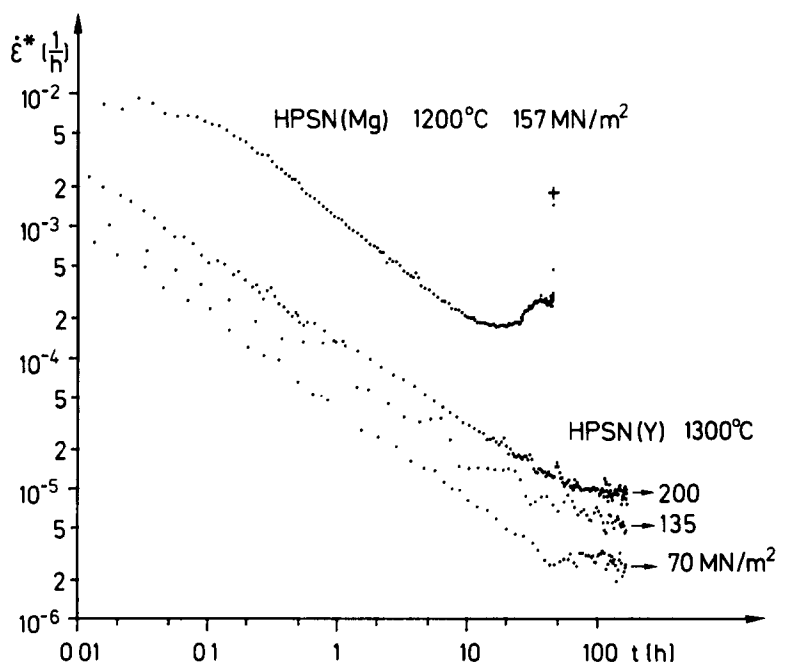

Fig. 3. Creep rate vs time for HPSN(Mg) and HPSN(Y) at different stresses σ^*.

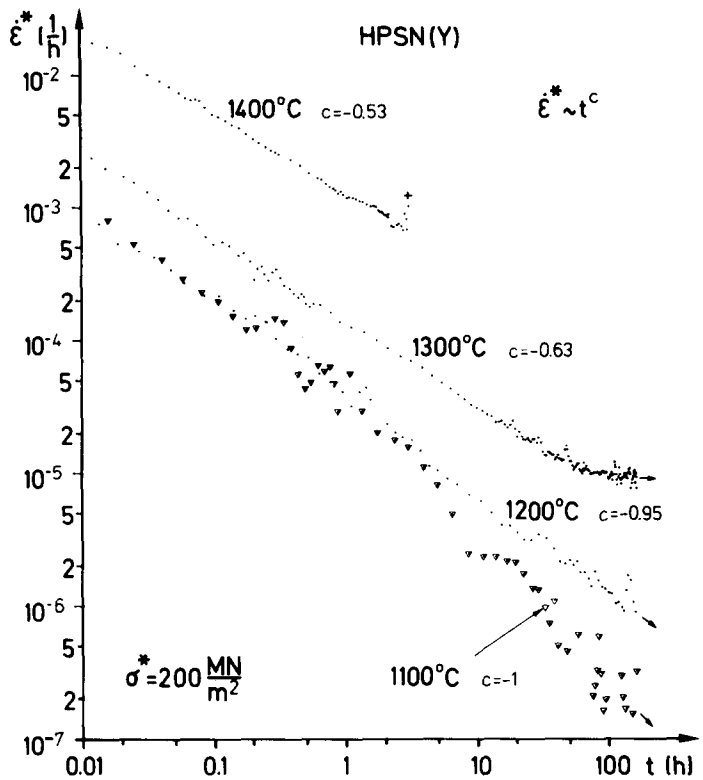

Fig. 4. Creep rate vs time for HPSN(Y) at different temperatures.

The relation between A^* and the uniaxial parameters A_t and A_c is:

$$2A^* = \left(\frac{2n+1}{6n}\right)^n \left\{A_t^{1/(n+1)} + A_c^{1/(n+1)}\right\}^{n+1} \tag{8}$$

which means that, if A_t is much greater than A_c, the bend deformation is controlled by tension creep.

An Arrhenius plot of A^* yields activation energies which correspond to those of pure SiO_2-glass in the case of HPSN(Mg) (560–700 kJ mol^{-1}) and with those of silica-glasses for HPSN(Y) (215 kJ mol^{-1}).[5] We would expect viscous grain boundary sliding to control the creep rate.

The ratio A_t/A_c can be determined by bend specimens with trapezoidal cross sections.[6,7] A_t/A_c has to be calculated from the different deformation velocities of two trapezoidal specimens with $M_2 = -M_1$. The results are listed in Table 2. HPSN(Mg) contains less grain boundary phase than HPSN(Y) and the softening temperature is lower. With increasing temperature (i.e. increasing softening of the grain boundary phase) n rises from 1 to 2, and simultaneously A_t becomes greater than A_c. It can be

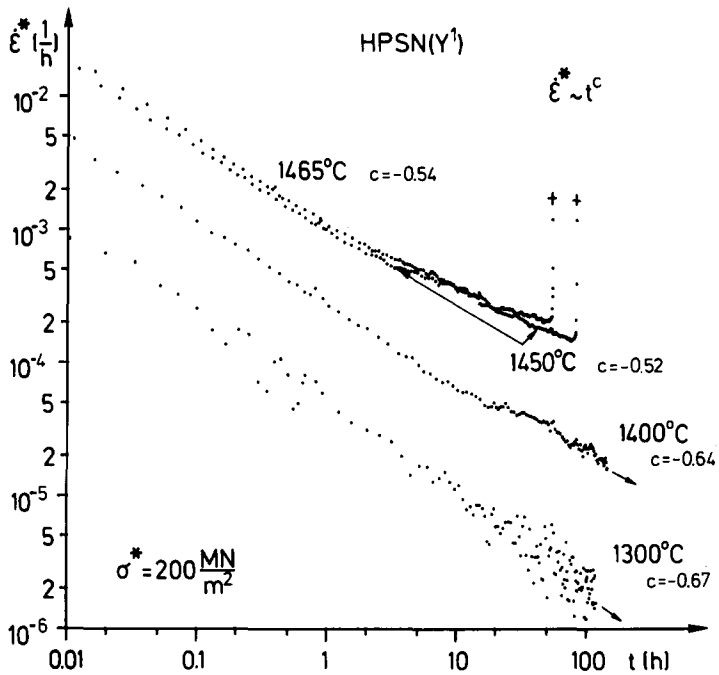

Fig. 5. Creep rate vs time for HPSN(Y¹) at different temperatures.

concluded that the ratio A_t/A_c, calculated for steady state conditions, is also valid for primary creep deformation. The ratio of the deflection rates $\dot{f}_{m1}/\dot{f}_{m2}$ from which A_t/A_c is calculated, or else the difference of their logarithmic values is time-independent (Fig. 6):

$$\dot{\varepsilon}(t) = A_1 \sigma^{n1} t^c \tag{9}$$

$$A_{1t}/A_{1c} \approx A_t/A_c, \qquad n_1 \approx n$$

This fact is to be taken into consideration when discussing the creep mechanisms (Section 4).

TABLE 2
Creep Data of the Studied Materials

	Y_2O_3 or MgO (wt. %)	T (°C)	n	A^* ($m^{2n}/MN^n h$)	A_t/A_c
HPSN(Y)	9·9	1 200	0·9[a]		3[a]
		1 300	1·2	$1{\cdot}9 \times 10^{-8}$	6
		1 400	1·5	$7{\cdot}7 \times 10^{-8}$	50
HPSN(Mg)	3·3	1 200	1·9	$1{\cdot}1 \times 10^{-8}$	100

[a] = calculated from primary creep data.

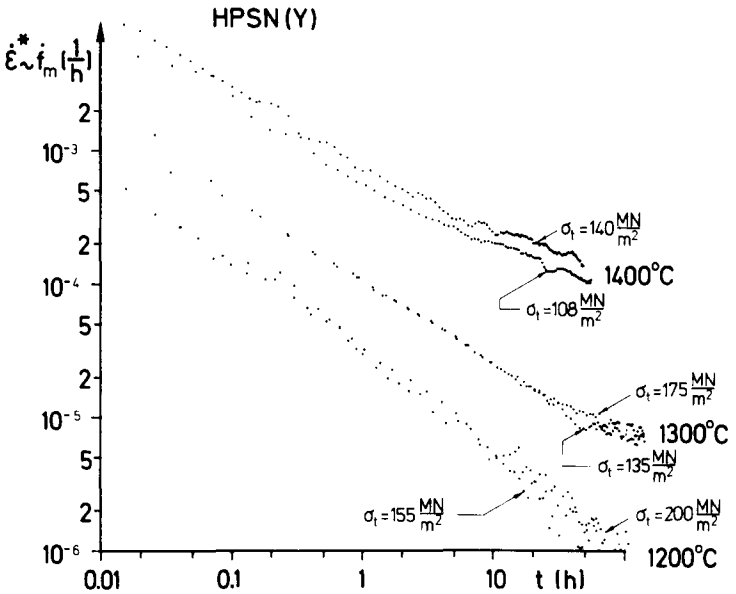

Fig. 6. Creep deformation of bend specimens with trapezoidal cross sections.

3.2 Elastic behaviour of a creep specimen

The elastic behaviour of a creep specimen during the creep test can be measured by partial unloading. In distinct time intervals, the load P is relaxed by 20% for a few seconds and is then reimposed. The ratio obtained $\Delta P/\Delta f_m$, is a measure for the specimen stiffness.

The HPSN(Y)-material exhibits a more or less distinct increase of $\Delta P/\Delta f_m$ with ε^* (Fig. 7), whereas HPSN(Mg) undergoes a decreasing $\Delta P/\Delta f_m$ up to $\varepsilon^* = 0{\cdot}4\%$ (Fig. 8).

Crystallization of the amorphous grain boundary phase and/or increasing grain linkage may stiffen the specimen, whereas creep porosity and crack growth may soften the specimen. As will be shown in Section 5 creep failure in HPSN(Mg), 1200°C, cannot actually be described without considering creep porosity. For HPSN(Y[1]) the following equation relating $\dot{\varepsilon}^*$ to the increase of stiffness can be established (Fig. 9):

$$\dot{\varepsilon}^* = \beta_0^* \left\{ \Delta \left(\frac{\Delta P}{\Delta f_m} \right) \right\}^{-k} \tag{10}$$

where k is an exponent and

$$\Delta \left(\frac{\Delta P}{\Delta f_m} \right) = \frac{\Delta P}{\Delta f_m} - \left. \frac{\Delta P}{\Delta f_m} \right|_{t=0}$$

Eqn 10 will be discussed in Section 4.

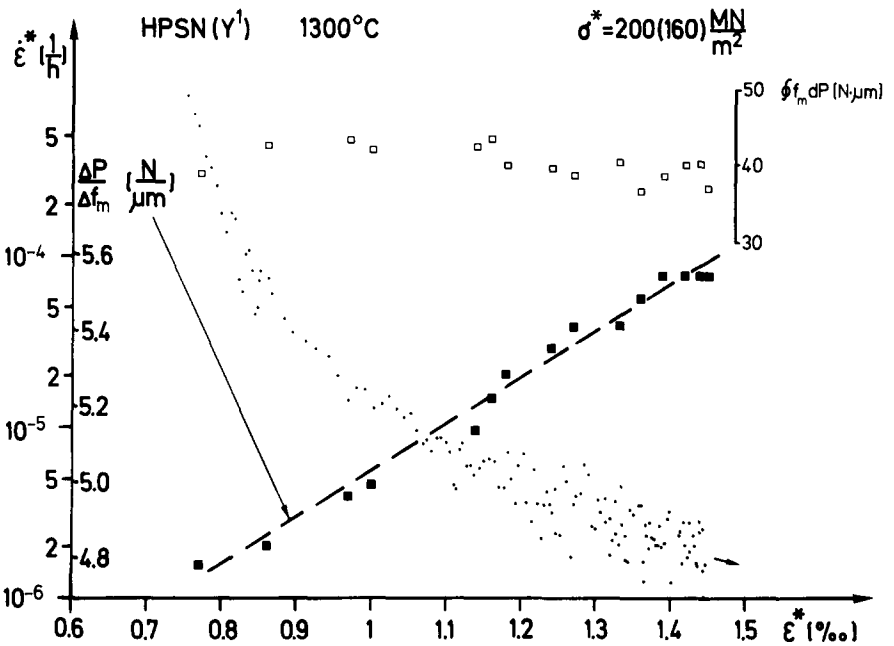

Fig. 7. Specimen stiffness, creep velocity and area of $P-f_m$-loop vs specimen deformation.

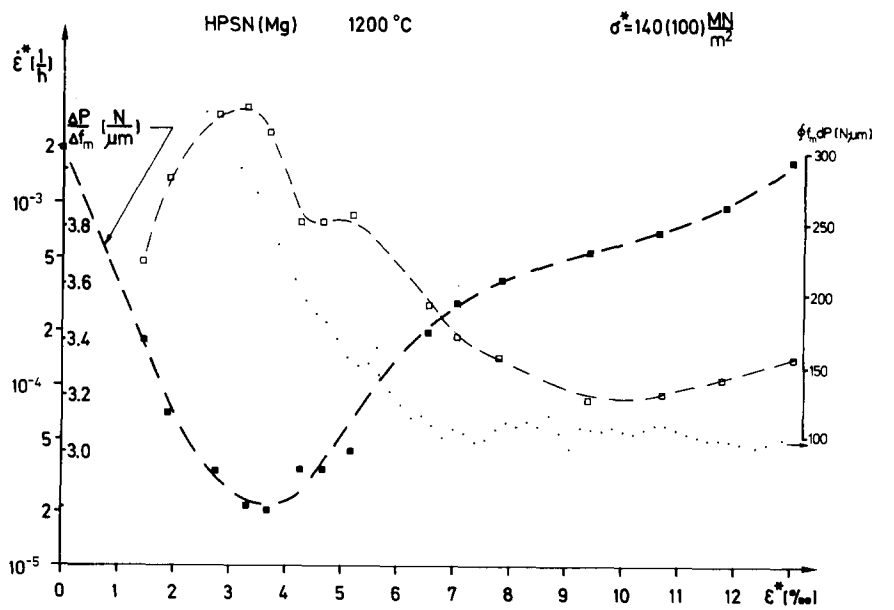

Fig. 8. Specimen stiffness, creep velocity and area of $P-f_m$-loop vs specimen deformation.

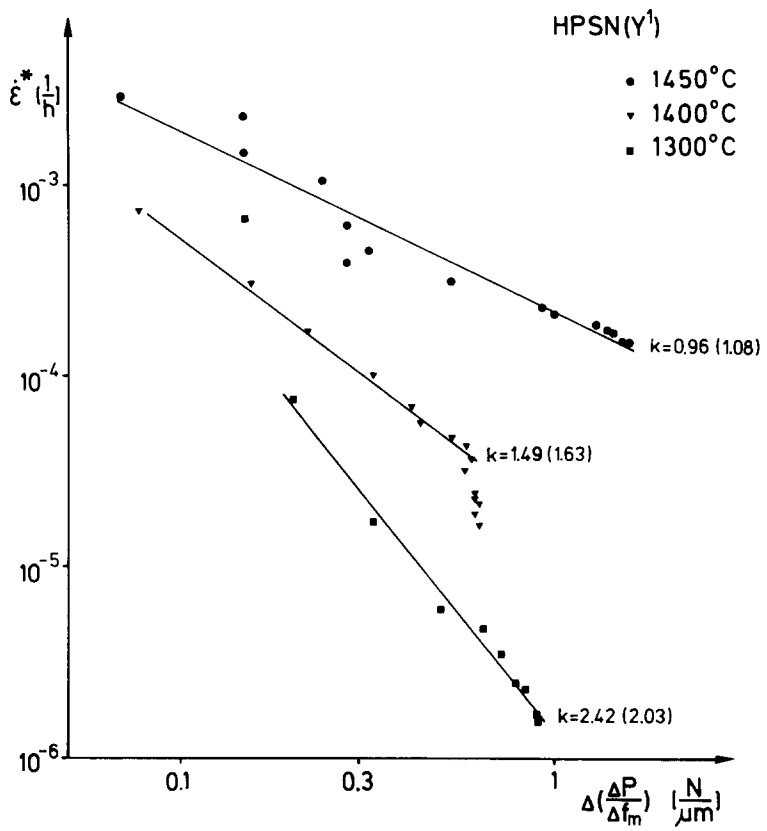

Fig. 9. HPSN(Y[1]): creep rate vs increasing specimen stiffness. The k-values in brackets are calculated, see Section 4.1.

3.3 Stress relaxation testing

To characterize a material, stress relaxation must also be considered. Usually the strain is held constant and the decreasing of stress is measured:

$$\dot{\varepsilon} = \frac{\dot{\sigma}}{E} + A|\sigma|^n \stackrel{!}{=} 0 \qquad A = \begin{cases} A_t, \sigma > 0 \\ -A_c, \sigma < 0 \end{cases} \tag{11}$$

In a bend test only the middle deflection f_m can be held constant. The decreasing of the bending moment is measured. For $A_t > A_c$ the time factor of the relaxation for tension is smaller than for compression. Tensile stresses relax quicker than compression stresses. Since the normal strength remains zero, the neutral axis will shift into the compression zone of the specimen. For $A_t \gg A_c$ this zone will disappear during the preceding creep test, so this case and the case $A_t = A_c$ are easy to calculate. We integrate eqn (11) over the

specimen height h and get:

$$n = 1: \qquad \frac{M}{M_0} = \exp(-A_t E t) \text{ valid for } A_t = A_c \text{ and } A_t \gg A_c \tag{12a}$$

$$n \neq 1: \qquad \frac{M}{M_0} = \frac{2n+1}{n} \int_0^1 u^{(n+1)/n} \left(\frac{t}{t_{0n}} F u^{(n-1)/n} + 1 \right)^{-1/(n-1)} \mathrm{d}u \tag{12b}$$

where $F = 1, u = \eta/2h$ for $A = A_t = A_c$, $F = 2^{1-n}, u = \eta/h$ for $A = A_t \gg A_c$ and $t/t_{0n} = (n-1)AE(\sigma^*(2n+1)/3n)^{n-1}t$.

In eqn 11 only stationary creep is considered. Time hardening can be described when introducing a fictitious time t^*, which is related to the real time t as follows:[8]

$$t^* = \frac{t^{1+c}}{1+c}$$

because $\mathrm{d}t^* = t^c \, \mathrm{d}t$, eqns (12a) and (12b) are also the solutions for a material undergoing time hardening creep

$$\dot{\varepsilon} = A\sigma^n t^c$$

if t in eqns (12a) and (12b) is replaced by t^*.

If strain hardening occurs

$$\dot{\varepsilon} = B\sigma^{n/(c+1)}\varepsilon^{c/(c+1)}$$

with $\varepsilon = (\sigma - \sigma_0)/E, \sigma/\sigma_0$ must be determined before integrating over the bend specimen height h to get M/M_0.

Figures 10 and 11 show the typical relaxation behaviour of HPSN: less relaxation occurs at lower temperatures. It does not depend on the height of the preliminary applied load, and it is postponed with extending duration of the preliminary creep test.

In the following, calculation and experiment are compared. The relaxation behaviour cannot be modelled by a creep n of 2 or 1·5, even if time hardening is taken into consideration. Assuming strain hardening would lead to a dependence of σ/σ_0 on σ_0 and therefore of M/M_0 on M_0 which in fact is not observed (Fig. 11). The statement

$$\dot{\varepsilon} = \frac{\dot{\sigma}}{E} + A\left(\frac{\sigma}{\sigma_0}\right)^{m_r} \sigma^n = 0 \tag{13}$$

leads to (with $n = 1$, because M/M_0 is not a function of M_0):

$$\frac{\sigma}{\sigma_0} = (1 + m_r A E t)^{-1/m_r} \tag{14}$$

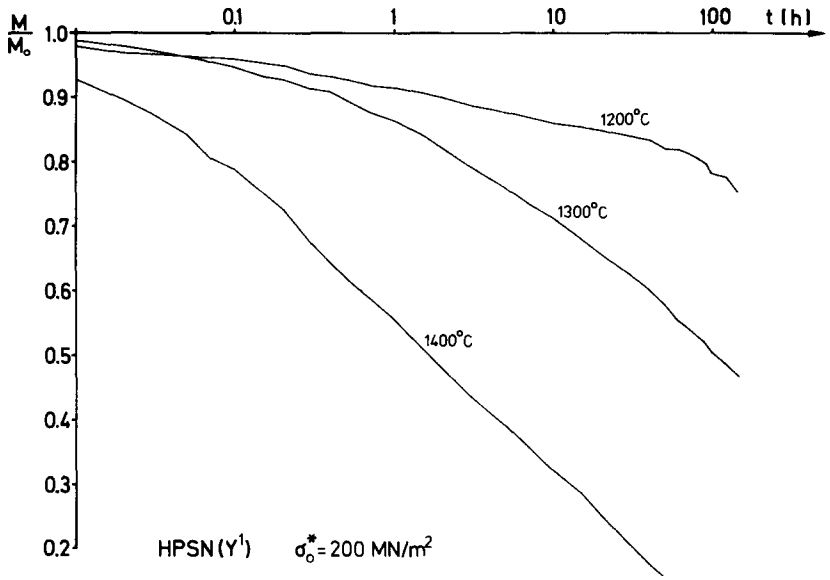

Fig. 10. Decreasing of the bending moment in the relaxation test at different temperatures.

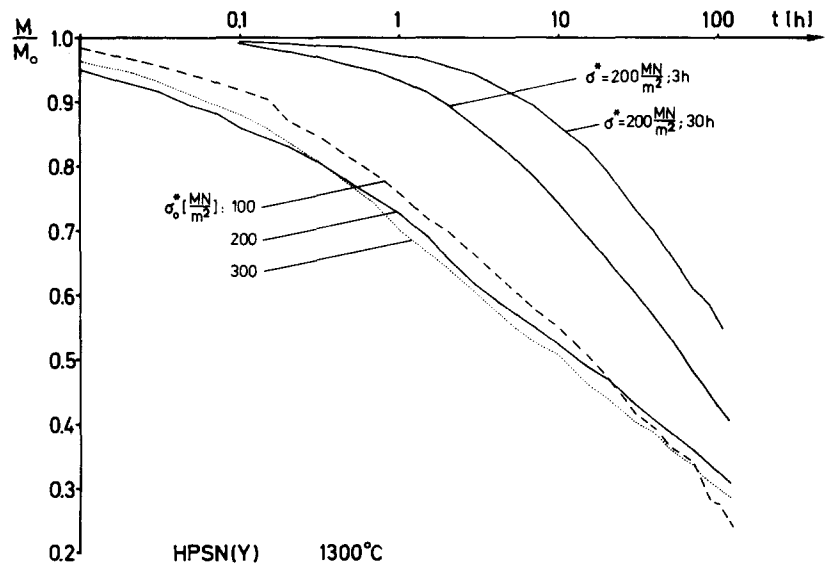

Fig. 11. Decreasing of the bending moment in the relaxation test at different starting loads and after different creep times.

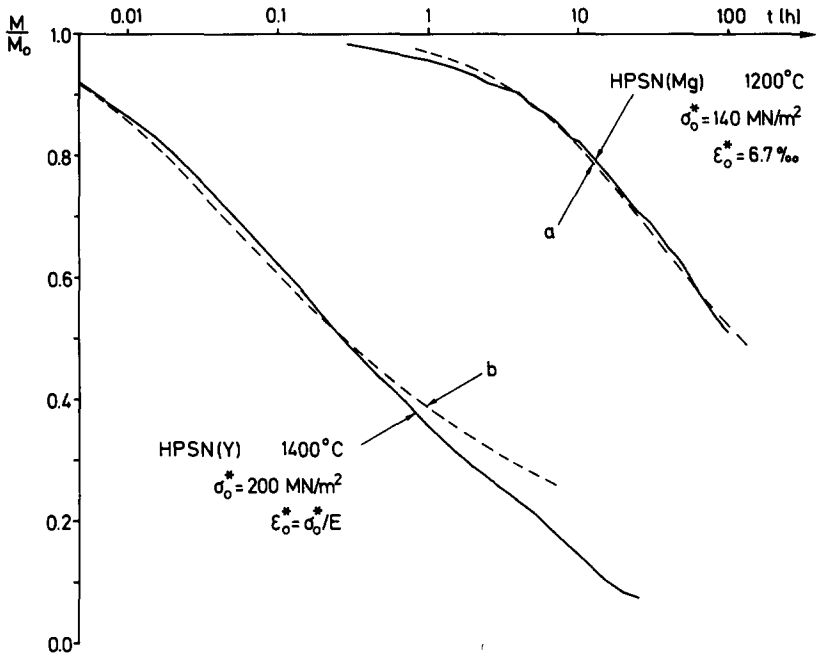

Fig. 12. Relaxation of the bending moment for constant middle deflection f_m, dashed lines are calculated from eqn (14a): (a), $m_r = 4$; (b), $m_r = 5$ (only the shape of the curves are compared, the relation of (a) and (b) to t is not considered).

For the cases $A = A_c$ and $A \gg A_c$ the bending moment M decreases in the same way as the stresses in the different fibres:

$$\frac{M}{M_0} = (1 + m_r AEt)^{-1/m_r} \tag{14a}$$

Best agreement is found with $m_r = 4$, HPSN(Mg) and $m_r = 5$, HPSN(Y) (Fig. 12).

Stress relaxation due to diffusion may be responsible for a faster decrease of M/M_0 for longer time periods than expected by eqn (14a).

In dynamic bend tests ($\dot{\sigma}^* > 0$) Fett *et al.*[9] determined a n-value of 7 for HPSN(Mg), 1200°C. How can these stress dependences ($n = 2, 7$; $m_r = 4$) be explained? An answer may be given in Section 4.

3.4. Time to rupture

The measured lifetimes of creep specimens are introduced and discussed in Section 5.

4 DISCUSSION: CREEP DEFORMATION

4.1 A structure model for creep

In Section 3.2 the creep rate was found to be

$$\dot{\varepsilon}^* = \beta_0^* \left\{ \Delta \left(\frac{\Delta P}{\Delta f_m} \right) \right\}^{-k} \tag{10}$$

where $\Delta(\Delta P/\Delta f_m)$ is the increase of the specimen stiffness during creep test.

For better understanding let us consider a mechanical two phase structure model, built up of elastically deformable grains which are surrounded by a viscous glassy phase. Si_3N_4 is covalently bonded and no yielding is expected even for temperatures at which the grain boundary phase softens. With increasing deformation of the whole structure the number, i, of grain contacts per unit volume (or else the grain linkage) will also increase. Let us assume the following relationship between increasing stiffness and increasing density of grain contact points:

$$\Delta \left(\frac{\Delta P}{\Delta f_m} \right) = \beta_1 \, \Delta i \tag{15}$$

The stress in the structure will be increasingly taken over by the contact points, and the viscous phase unloaded. Only a viscous phase in motion transmits a shearing stress. The creep rate $\dot{\varepsilon}$ is proportional to an average sliding rate $\dot{\gamma}$:

$$\frac{\dot{\varepsilon}}{\beta'} = \dot{\gamma} = \frac{\tau}{\eta} \tag{16}$$

Where η is the viscosity and the average shear stress τ is assumed

$$\tau = \beta_2 \left(\frac{1}{\Delta i} \right)^k \tag{17}$$

At high temperature and high viscosity $k = 1$. With decreasing temperature the boundary phase becomes more tenacious, loses its flow capacity and acts as additional contact points: $k > 1$. From this we find eqn (10):

$$\dot{\varepsilon} = \beta' \dot{\gamma} = \beta' \frac{\tau}{\eta} = \frac{\beta' \beta_2}{\eta} (\Delta i)^{-k} = \frac{\beta' \beta_2 \beta_1^k}{\eta} \left\{ \Delta \left(\frac{\Delta P}{\Delta f_m} \right) \right\}^{-k} \tag{10a}$$

For the simple case that the stiffness increases linearly with the deformation ε (e.g. observed for HPSN(Y[1]), 1300°C, (Fig. 7))

$$\Delta\left(\frac{\Delta P}{\Delta f_m}\right) = \beta_3 \varepsilon \tag{18}$$

Introducing eqn (10a)

$$\left(\frac{\dot{\varepsilon}}{\beta_0}\right)^{-1/k} = \beta_3 \varepsilon; \qquad \beta_0 = \frac{\beta' \beta_2 \beta_1^k}{\eta}$$

rearranging and after integration

$$\varepsilon = \{(k+1)\beta_0 \beta_3^{-k}\}^{1/(k+1)} t^{1/(k+1)}$$

or else

$$\dot{\varepsilon} \sim t^{-k/(k+1)} = t^c, \qquad \frac{1}{k+1} - 1 = c \tag{19}$$

Thereby the relationship to the primary creep kinetics is established. At high temperatures $k = 1$ and $c = -0{\cdot}5$. With diminishing temperature k increases ($k > 1$) while c approaches -1. The k-values in brackets in Fig. 9 are calculated from eqn 19 (c-values are taken from Fig. 5) and are in agreement with the experimental determined k.

The decreasing of the creep velocity during the primary range can thus be described by a mechanical two phase model. Other models to be found in the literature,[4,10] following the Kingery sintering model, consider solution/reprecipitation of grain substance as rate controlling. These models predict an exponential stress dependency of the creep rate, which in fact is not observed.

It is doubtful whether creep mechanisms can be deduced from simple structure models like that of Lange.[11] The stiffness of his cubic–grains–structure will decrease with increasing deformation. This is not observed, not even in HPSN(Mg).

Grain contact points can be removed by diffusion or, depending on the movement of the grains relative to each other, the contact area may increase. If an equilibrium between added and removed contact points is reached, stationary creep rates will result. That means, by transition from primary to secondary creep, a change in the creep rate controlling factor occurs (first grain boundary sliding restrained by rising number of grain contact points—then removal of these contact points by diffusion).

The asymmetric creep behaviour is therefore probably independent of the creep mechanism, since it is observed in the same manner during primary and secondary creep.

4.2 Void nucleation and growth—reason for asymmetrical creep

When the stress exceeds a limit voids or microcracks nucleate in the grain boundary phase between the grains at propitious sites. The limit depends on the degree of the local inhomogeneity. We assume that the number of microcracks per unit volume, $\tilde{N}$, may be described by a power law:

$$\tilde{N} = \beta_D \sigma^m \tag{20}$$

i.e. σ^{m-1} describes the defect size distribution in the unloaded structure. Voids and microcracks grow in accommodation to the creep deformation (they do not influence the creep kinetics but are indispensable for the complex mechanism of creep). This can be shown by cooling a specimen after a creep test without removing the load, and by reapplying the same bending moment, but of opposite sign, in a second test. The creep kinetics are the same, with the exception of the values of the creep rates; in the second test they are somewhat higher (Fig. 13). The voids and microcracks now present in the compression zone close and therefore contribute to the deformation by grain boundary sliding.

In creep test with constant loading, voids and microcracks nucleate at the start of the test during application of the load. Subsequently, voids or cracks may occur if adjacent plastic deformation is hindered, e.g. by a very large

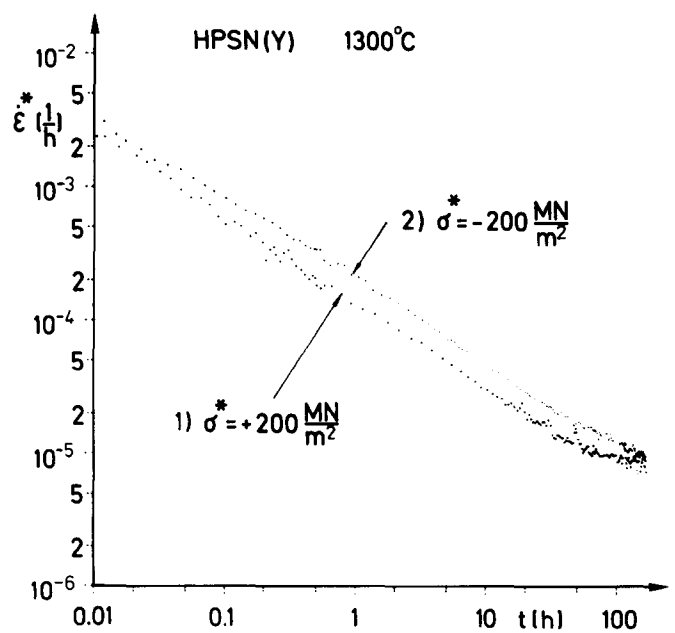

Fig. 13. Creep kinetics of HPSN(Y): (1) = conventional test, (2) = second test with the same specimen, but with opposite sign of the bending moment.

grain. The nucleation of voids accelerates the creep rate. From this statement the following hypothesis can be proposed (for uni-axial tensile stress):

$$\dot{\varepsilon} = \left(1 + \beta_N \frac{\mathrm{d}\tilde{N}}{\mathrm{d}t}\right) A(t)\sigma^n \tag{21}$$

whereas (eqn 20)

$$\frac{\mathrm{d}\tilde{N}}{\mathrm{d}t} = \beta_D \sigma^{m-1}\dot{\sigma} \tag{22}$$

Hypothetically (to observe this effect) we need an increasing stress rate. For sufficiently high $\dot{\sigma}$ (so that $1 \ll \beta_N \, \mathrm{d}\tilde{N}/\mathrm{d}t$) it follows from eqn 21 (with $\sigma = \dot{\sigma}t$):

$$\dot{\varepsilon} \sim \dot{\sigma}^{n+m} \tag{23}$$

For HPSN(Mg), 1200°C, $n + m = 7$.[9]

During stress relaxation (see Section 3.3) viscous or Newtonian grain boundary sliding is responsible for the stress decrease: therefore $n = 1$ in eqn 13. When the stress decreases, the smaller voids or cracks will close if the arrangement of the surrounding grains is favourable. Only a certain

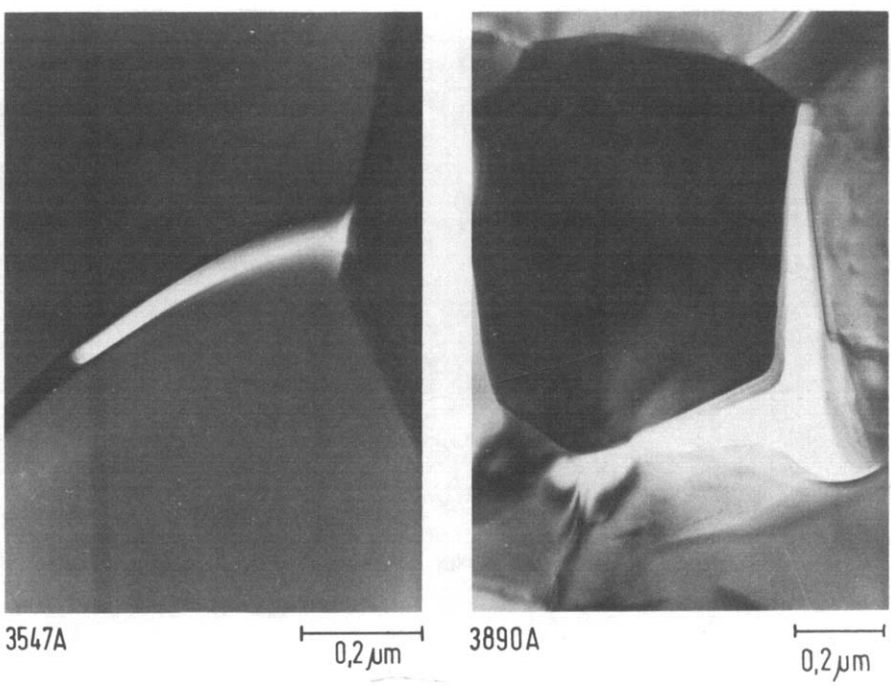

Fig. 14. TEM-micrographs of creep porosity in: (a), HPSN(Mg); and (b), HPSN(Y), $\varepsilon^* = 1\%$.

percentage of the voids of a size group will disappear. Surface energy will be recuperated and the specimen reverts to a more stable state.

On the other hand, voids which close slacken the stress relaxation because the volume of the voids must be compensated either by elastic strain or by plastic deformation. The 'tighter' the void size distribution is (high value of $m-1$) the slower the stress can relax. It can be expected that the size distribution of voids in the deformed structure and of defects in the preliminary structure respectively is similar. The more σ decreases below σ_0, the more voids will close; voids which should, due to their size, already have disappeared but were hindered by the surrounding grains. This will slow down the stress decrease. This might be the reason why stress relaxation can be described well by eqn 14 with $m-1=m_r=4$ for HPSN(Mg).

The creep must be asymmetrical because of the different tendency of nucleating voids or microcracks, depending on whether the structure is submitted to tensile or to compressive stresses. Voids and microcracks easily nucleate under tension, which favour grain boundary sliding, and yield a contribution to the creep deformation. Figure 14 shows creep porosity, originating in the outer tensile zone of the bend specimen. At similar deformation ($\varepsilon^* = 1\%$) much less porosity is observed in HPSN(Y) than in HPSN(Mg). In both cases crystallisation of the amorphous phase could not be detected.

5 SLOW CRACK GROWTH

5.1 Theory

The following statement can be made on the slow crack growth in an HPSN structure, submitted to creep deformation. With our apparatus it is not possible to observe or to measure directly the growth of a crack. We determine, for example, the time to failure which allows an indirect study of the crack growth kinetics. The specimen were precracked by Knoop indentation or by notch, opening modus is *I*.

Griffith[12] considers the energy conversion in a linear–elastic solid exhibiting crack lengthening by *da*:

$$\mathrm{d}W - \mathrm{d}U = 2\gamma b\,\mathrm{d}a \tag{24}$$

where W is the work done by the external force, U is the elastic energy stored and $2\gamma b\,\mathrm{d}a$ the provided surface energy. The Griffith criterion indicates whether crack lengthening is thermodynamically possible. Additionally the stresses at the crack tip must exceed the cohesive strength (for more details see Ref. 13). If they do not, the bonding may be overcome by thermal

fluctuation, or a chemical attack may weaken the bonding strength. The so-called stress criterion loses its significance in materials undergoing creep or viscous flow. The decohesion therefore cannot be stopped. Crack growth will occur wherever the free energy of the specimen is lowered.

Consider a specimen with only one crack. If the crack does not grow, the work done by the external forces will be consumed as creep work. The greater part will be converted to heat, but some will be stored as surface energy in form of voids or microcracks or as elastic energy by increasing grain linkage.

If crack growth is considered to be a discreet event, it is governed by the following extended energy balance:

$$\mathrm{d}W - \mathrm{d}U \overset{(\geq)}{=} \mathrm{d}W^* + 2\gamma b\,\mathrm{d}a + \mathrm{d}q \tag{25}$$

where q is the energy dissipation by plastic deformation at the crack tip which was first taken into account by Orowan and Irwin; W^* is the released energy, preliminarily trapped by creep. W^* supports a crack extension. W^* may be stored as surface energy of the voids or microcracks through which the crack grows. The extended energy balance in eqn (25) leads to:

$$G - 2\gamma - \frac{\mathrm{d}q}{b\,\mathrm{d}a} + \frac{\mathrm{d}W^*}{b\,\mathrm{d}a} \overset{(\geq)}{=} 0 \tag{26}$$

For linear–elastic material behaviour the energy release rate G is related to the stress intensity factor; for crack opening modus I:

$$G = \frac{K_I^2}{E'}, \qquad E' = \frac{E}{1 - \nu^2} \tag{27}$$

If no surplus of preliminary stored creep deformation energy is needed to fulfill the energy balance, crack growth is unstable, $\mathrm{d}W^* = 0$:

$$2\gamma + \left.\frac{\mathrm{d}q}{b\,\mathrm{d}a}\right|_{a=a_c} = \frac{K_{IC}}{E'} \tag{28}$$

(K_{IC} is the critical stress intensity factor). If crack growth is energetically favourable, it can be described by

$$\frac{\mathrm{d}W^*}{b\,\mathrm{d}a} \overset{(\geq)}{=} \frac{1}{E'}(K_{IC}^2 - K_I^2) \tag{29}$$

A similar statement is considered by Dutton for crack growth by diffusion.[14] A crack expands if the free energy F of the specimen is thereby lowered: $\mathrm{d}F/\mathrm{d}a \leq 0$.

In the following W^* is assumed to be internal surface energy accumulated by creep.

$$\mathrm{d}W^* = 2\gamma\,\mathrm{d}O \tag{30}$$

Where O is the surface of voids and microcracks through which the crack grows.

As previously mentioned (Section 4.2), the void or microcrack density can be expressed in terms of a power law:

$$\tilde{N} \sim \sigma_e^m \tag{20a}$$

σ_e is the effective stress. Void or microcrack growth occurs in accommodation to the creep deformation:

$$\dot{V} \sim \dot{\varepsilon}_e = A\sigma_e^n, \qquad n = 1 \ldots 2 \tag{31}$$

According to von Mises, σ_e can be calculated by the stress deviator s_{ij}:

$$\sigma_e = \sqrt{\frac{3}{2} s_{ij}^2} \tag{32}$$

For linear–elastic material behaviour in the vicinity of a crack tip $\sigma_e = \sigma_{e,0}$:

$$\sigma_{e,0} = \frac{K_I}{\sqrt{2\pi r}} \cos\frac{\varphi}{2} \sqrt{(1-2\nu)^2 + 3\sin^2\frac{\varphi}{2}} \tag{33}$$

where r, φ are polarcoordinates. For a bending beam the stress intensity factor is:

$$K_I = \sigma\left(\frac{h}{2}\right)\sqrt{a}\,Y \tag{34}$$

where Y is a geometrical function,[15] a the crack length, and $\sigma(h/2)$ the outer tensile stress of the bend specimen. During creep its value decreases to 50% of the initial height (Section 2). The stresses at the crack tip also decrease with time. This might be described by a function $F(t)$:

$$\sigma_e(t) = \sigma_{e,0} F(t), \qquad \text{e.g. } n = 1\text{: } F(t) = \exp(-A_t E t) \tag{35}$$

If a stress field is displaced with a constant velocity, for example in front of a crack, it is smallest at the lowest velocity. At a distance x_1 in front of the crack tip one obtains ($\varphi = 0$):

$$\sigma_e(x_1) = \int_{\infty}^{x_1} \frac{\partial \sigma_{e,0}}{\partial x} F\left(\frac{x}{\dot{a}} - \frac{x_1}{\dot{a}}\right) \mathrm{d}x \tag{36}$$

$$\approx \frac{K_I(1-2\nu)}{\sqrt{2\pi x_1}} \exp\left(\frac{-3A_t E x_1}{2(1+\nu)\dot{a}}\right) \tag{36a}$$

Because of the stress concentration at the crack tip, new voids and microcracks are nucleated and therefore the effective stress does not exceed a limit $\sigma_{e,max}$ (Fig. 15). Consequently a damage zone, ρ, exists in front of a crack tip. The extension of ρ is a measure of the stress intensity. In analogy to

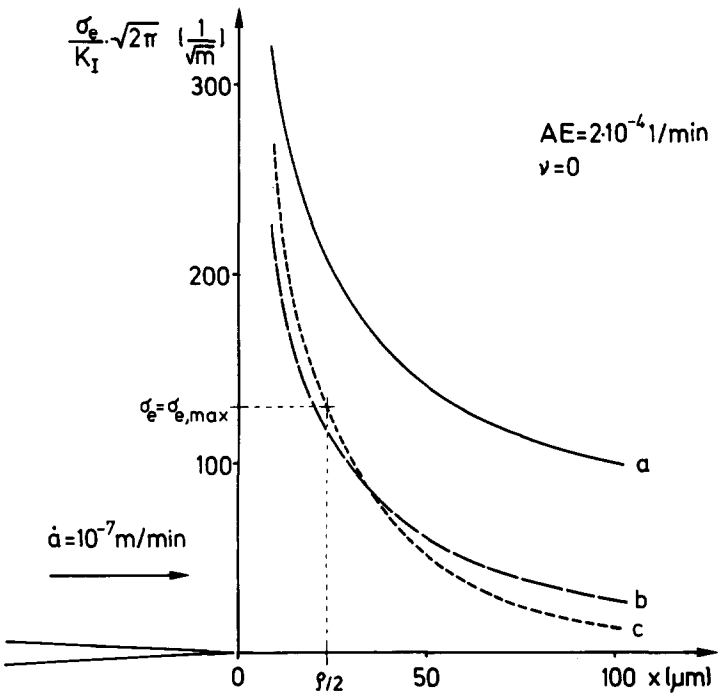

Fig. 15. Effective stress in front of a slowly growing crack: (a), linear-elastic case; (b), eqn (36) and; (c) eqn (36a).

the extension of the plastic zone in metals: $\sigma_{e,max} = \sigma_e(x_1 = \rho/2)$. If $F(t)$ can be represented by an exponential function, a first approximation to determine ρ leads to a transcendental equation:

$$\ln \rho + \frac{A_t E \rho}{\dot{a}} = \ln \frac{K_I^2}{\pi \sigma_{e,max}} \tag{37}$$

where ρ is measured in the crack plane. The new porosity V_ρ, originating in the damage zone, can be calculated:

$$V_\rho = \tilde{P}_1 \int_0^{t_1} \tilde{N} \dot{\varepsilon}_e \, dt \tag{38}$$

Where t_1 is the time the crack of velocity $\dot{a}$ needs to travel a distance ρ:

$$t_1 = \frac{\rho}{\dot{a}} \tag{39}$$

$\dot{\varepsilon}_e$, an effective creep rate

$$\dot{\varepsilon}_e = A_t \sigma_e^n \tag{7a}$$

and $\tilde{N}$ is the void or microcrack density

$$\tilde{N} = \tilde{P}_2 \rho^q \tag{40}$$

(the exponent q will be determined later). Here $\tilde{N}$ should be related to the strain at the crack tip which is proportional to ρ.

The value of $\dot{a}$ is obtained from energy balance (eqn 29) as shown in the following. Voids and microcracks, already present in the structure, will extend under creep conditions:

$$V_\varepsilon = V_0 \left(1 + \int_0^t \dot{\varepsilon}\, \mathrm{d}t \left(1 + \int_0^{t_1} \dot{\varepsilon}_e\, \mathrm{d}t\right)\right) \tag{41}$$

where V_0 is the porosity after loading, t the time measured from the beginning of the creep test and $\dot{\varepsilon}$ the creep rate.

Assuming, the shape of the cavities to be crack like with an average width d, then the internal surface is proportional to the hollow volume. The pre-existing surface, when the crack propagates by bda, is (with eqn 30):

$$\frac{1}{d}(V_\rho + V_\varepsilon) = \frac{\mathrm{d}O_c}{bda} = \frac{1}{\gamma}\frac{\mathrm{d}W^*}{bda}, \qquad O_c = 20 \tag{42}$$

V_ρ and V_ε are the hollow volumes per unit area. Introducing eqns (38), (41) (considering eqns (39), (40) and (7a) and (29) in eqn (42) the crack growth rate, $\dot{a}$, can be deduced ($K_{IC}^2/E' - V_0\gamma/d$ is the theoretical value of the porefree material and is replaced in the following by K_{IC}^2/E' which is measurable):

$$\dot{a} = \frac{\alpha_a \rho^{q+1} + \alpha_b \rho \varepsilon}{\dfrac{K_{IC}^2}{E'} - \dfrac{K_I^2}{E'} - \alpha_c \varepsilon} \tag{43}$$

($\alpha_a = \tilde{P}_1 \tilde{P}_2 A_t \sigma_{e,\max}^n \gamma/d$, $\alpha_b = V_0 A_t \sigma_{e,\max}^n \gamma/d$, $\alpha_c = \gamma V_0/d$). ρ is to be taken from eqn 37. In a bend specimen the strain $\dot{\varepsilon}$ of the fibre at the crack tip is proportional to the distance of that fibre to the neutral axis. For approximation $\dot{\varepsilon}$ in eqn (41) is the secondary creep velocity: $\dot{\varepsilon} = D(h_t - a)$. It follows:

$$\dot{a} = \frac{\alpha_1 \rho^{q+1} + \alpha_2 \sigma^{*n} t (h_t - a)\rho}{\dfrac{K_{IC}^2}{E'} - \dfrac{K_I^2}{E'} - \alpha_3 \sigma^{*n} t (h_t - a)} \tag{43a}$$

($\alpha_1 = \alpha_a$, $\alpha_2 = \alpha_b A^* 2/h$, $\alpha_3 = \alpha_c A^* 2/h$). α_1, α_2 and α_3 contain geometrical factors and material factors. If no creep damage in the specimen occurs: $\alpha_2 = \alpha_3 = 0$. For $\dot{a} \gg A_t E \rho$ it is $\rho \sim K_I^2$ (eqn 37) and q can be estimated ($\tilde{N} \sim \rho^q \sim K_I^{2q} \sim \sigma_e^{2q} = \sigma_e^m$):

$$q \approx \frac{m}{2} \tag{44}$$

with $m-1$ characterizing the void or microcrack size distribution $m-1$ is supposed to describe the stress decrease in the relaxation test (Sections 3.3 and 4.2).

5.2 Crack growth in HPSN(Mg)

With eqns (43) and (37), theory and experiment can be compared. Most of the values needed to determine the α's (see Table 3) can be taken from creep data or are geometrical factors. The starting crack length a_0 of natural flaws is taken from literature,[16] a_0 of Knoop-indentation pre-crack was measured on the broken surface. For HPSN(Mg), 1200°C $m = m_r + 1 = 5$ (Fig. 12) and therefore $q = 2{\cdot}5$. By proceeding numerically step by step, increasing a by

TABLE 3
Numerical Data for HPSN(Mg), 1200°C to Calculate $\dot{a}$ from eqns (37) and (43)

K_{IC}	15	$MN/m^{3/2}$
$\sigma_{e,max}$	200	MN/m^2
q	2·5	
$\alpha_1 E'$	3×10^9	$MN^2/m^{5\cdot5}$ min
$\alpha_2 E'$	4×10^{-8}	$1/min^2$
$\alpha_3 E'$	1×10^{-3}	1/min
$A_t E'$	2×10^{-4}	m^2/MN min

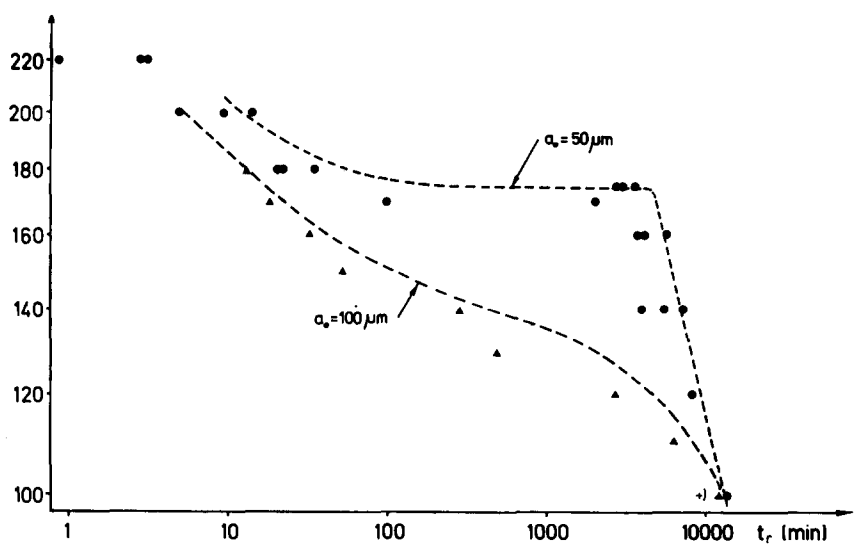

Fig. 16. Stress rupture diagram for HPSN(Mg), dashed lines are calculated (numerical data, see Table 3).

$\dot{a} \times \Delta t$ until K_{IC} is reached, the rupture time at a given nominal stress σ^* can be computed. Figure 16 shows the results and the experimental data. The big difference in rupture time t_r for $a_0 = 50\,\mu m$ (natural flaws) between $\sigma^* = 170$ and 180 MN m^{-2} originates in the relaxation of the outer tensile stress of the bend specimen. The stress intensity also decreases. For short initial crack lengths the crack velocity is small; additionally the effective stress σ_e in front of the crack tip is lowered by creep, requiring time. The crack leading to failure will stop propagating until creep damage in the whole specimen will allow it to start again. Failure occurs within a short time. Rupture behaviour can also be described by the Monkman–Grant equation:[12] $\varepsilon^* \sim 1{\cdot}7\%$. For bigger initial crack sizes a_0 (e.g. 100 μm) this effect is not large. At low stresses the difference in rupture time between pre-cracked and undamaged specimens is small. Because of the scattering of the structure properties and the high number of natural flaws, a pre-cracked specimen does not in all cases break at the artificial pre-crack.

Figure 17 shows the crack velocity in dependence on time for a precracked specimen. To check this result, a specimen was cooled without removing the load after 20 min and another after 12 hours of creep test. They were broken at room temperature. Figure 18 demonstrates that the crack extension zone is of similar size in both cases. Between these two points in time, $\dot{a}$ decreases by several orders of magnitude. The damage zone ρ is shown in Fig. 19. The notched specimen was cooled down under load, the oxide layer was removed and the photograph taken.

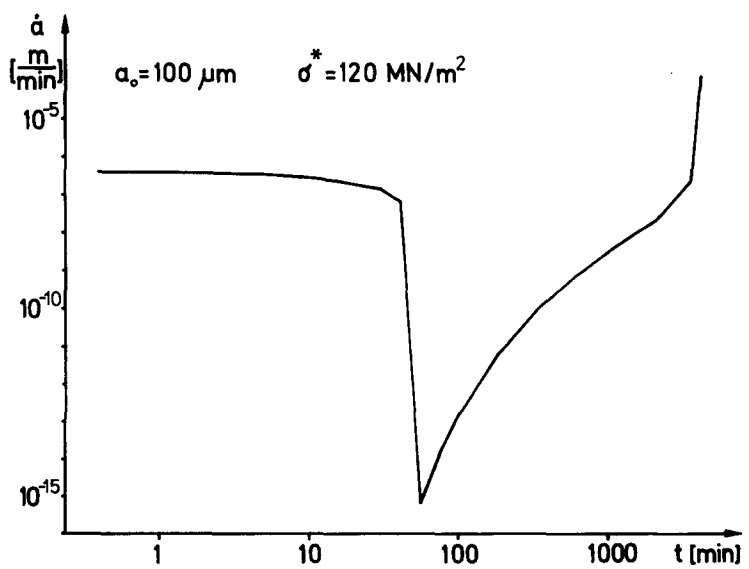

Fig. 17. Crack velocity vs time, calculated for HPSN(Mg), 1200°C.

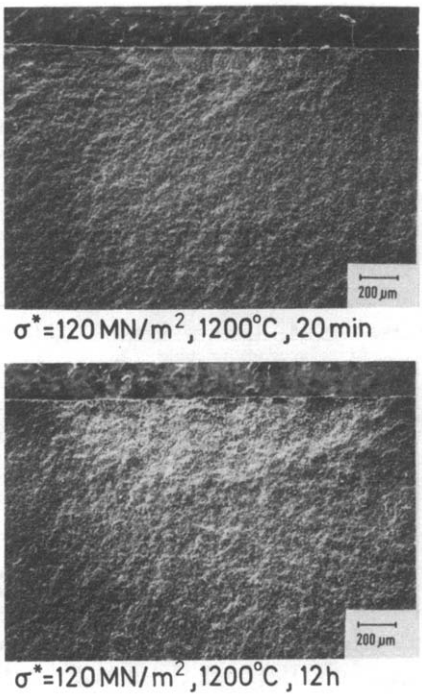

Fig. 18. HPSN(Mg)-fracture surface, 5 Knoop indentations (49 N), after creep test in air fractured at room temperature (SEM).

HPSN(Mg) was also tested in vacuum. At a pressure of only some 10^{-6} mbar the grain boundary phase volatilizes (Fig. 20). This leads to an enhanced crack growth rate. Beside the hollow volume a constant contribution in the energy eqn (29) must be taken into consideration:

$$\alpha_4 \frac{\mathrm{d}t}{\mathrm{d}a} + \gamma \frac{\mathrm{d}O_c}{bda} = \frac{\mathrm{d}W^*}{bda} = \frac{1}{E'}(K_{IC}^2 - K_I^2) \tag{45}$$

Analogous to the procedure shown before we get:

$$\dot{a} = \frac{\alpha_1 \rho^{q+1} + \alpha_2 \sigma^{*n} t(h_t - a)\rho + \alpha_4}{\frac{K_{IC}^2}{E'} - \frac{K_I^2}{E'} - \alpha_3 \sigma^{*n} t(h_t - a)} \tag{46}$$

With the exception of α_4, all factors are taken from calculation in air. A better agreement between calculation and experiment is possible by enlarging a_0: natural flow from 50 to 70 μm, Knoop indentation precracks from 100 to 140 μm (Fig. 21). This points to the fact that flaws exhibit a certain amount of healing in an oxidizing atmosphere.

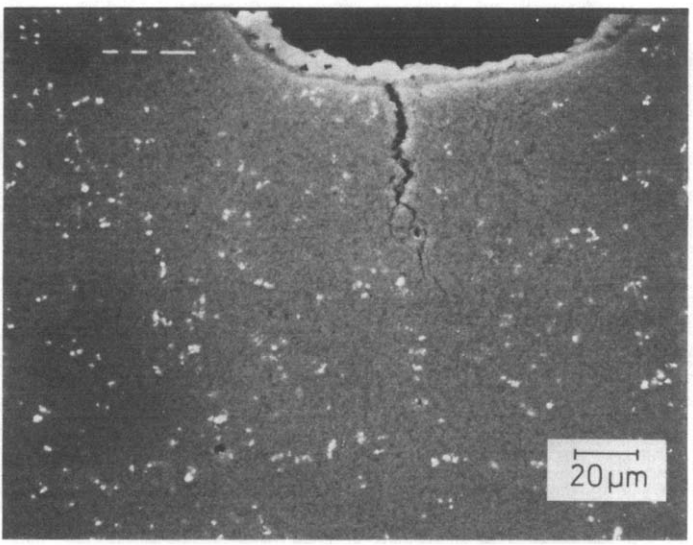

(a)

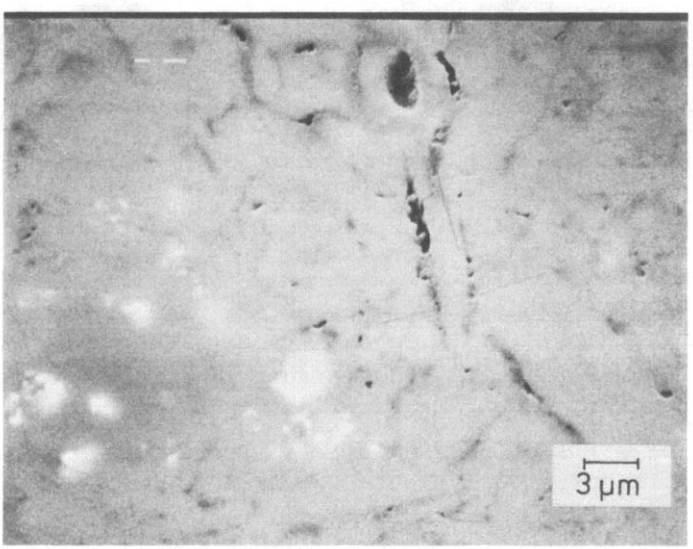

(b)

Fig. 19. SEM-micrographs of the damage zone in a notched HPSN(Mg) specimen.

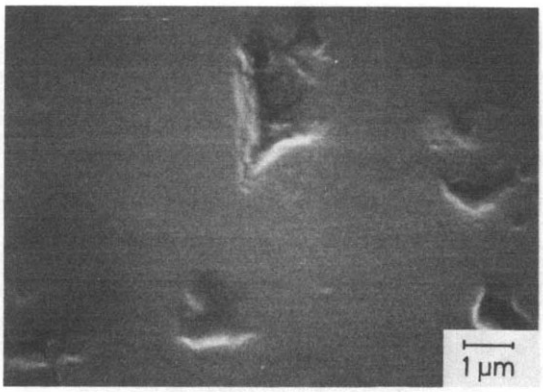

(a)

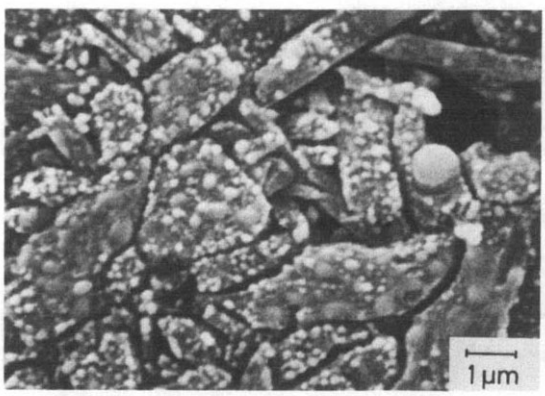

(b)

Fig. 20. SEM-micrographs of the polished surface of HPSN(Mg): (a), before; and (b), after treatment in vacuum (3 h, 1200°C, 3×10^{-6} mbar).

5.3 Crack growth in HPSN(Y)

HPSN(Y) was tested under static and cyclic loading conditions. This HPSN-material with 9·9 wt% Y_2O_3 additive does not experience much creep damage at 1400°C. Stiffness does not decrease with the deformation, and only a few voids and microcracks can be observed by TEM (see section 4): $V_0 \approx 0$, i.e. $\alpha_2 = \alpha_3 = 0$. Rupture times in these experiments are not particularly long, so the decreasing of σ_e in front of the crack tip by creep may be neglected. Thus eqn (43) can be simplified:

$$\dot{a} \sim \rho^{q+1} \sim K_I^N \tag{47}$$

with $N \approx 8$ following the hypothesis of Section 4.2; from eqn (44): $N = m + 2$, $m = m_r + 1 = 6$ (Fig. 12).

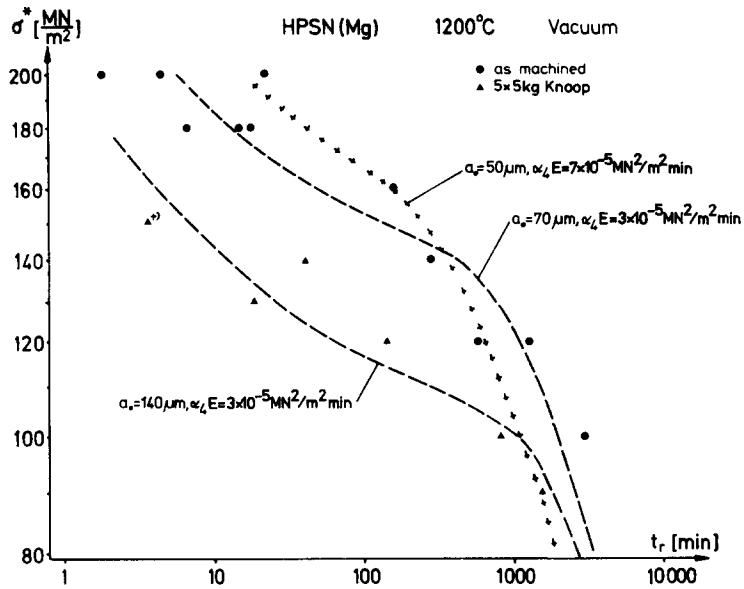

Fig. 21. Stress rupture diagram for HPSN(Mg), dashed lines are calculated.

With $N = 8$, it is possible to predict time to failure under cyclic load from static data. It is assumed that crack growth mechanism remains the same (the same crack growth rule is valid). Furthermore, it is supposed that the outer tensile stresses decrease with time under static and cyclic load in the same manner. The stress lowering leads to a fictitious rupture time t_r^*, which can be expected if the outer tensile stress would remain constant:

$$t_r^* = \int_0^{t_r} \left(\frac{\sigma\left(\left(\frac{h}{2}\right), t\right)}{\sigma^*} \right)^N \mathrm{d}t \tag{48}$$

Notch depth of the specimens is 0·1 mm. The results are shown in Fig. 22 (for more details concerning theoretical treatment see Ref. 17).

6 CONCLUDING REMARKS

A Griffith energy balance, extended by W^*, leads to an equation for the crack velocity. Voids and microcracks nucleated in the stress field at the crack tip and in the whole creeping specimen are considered to facilitate crack propagation. Experiments are in agreement with theoretical calculations. A relationship also exists between the crack growth exponent N and the stress relaxation under constant strain.

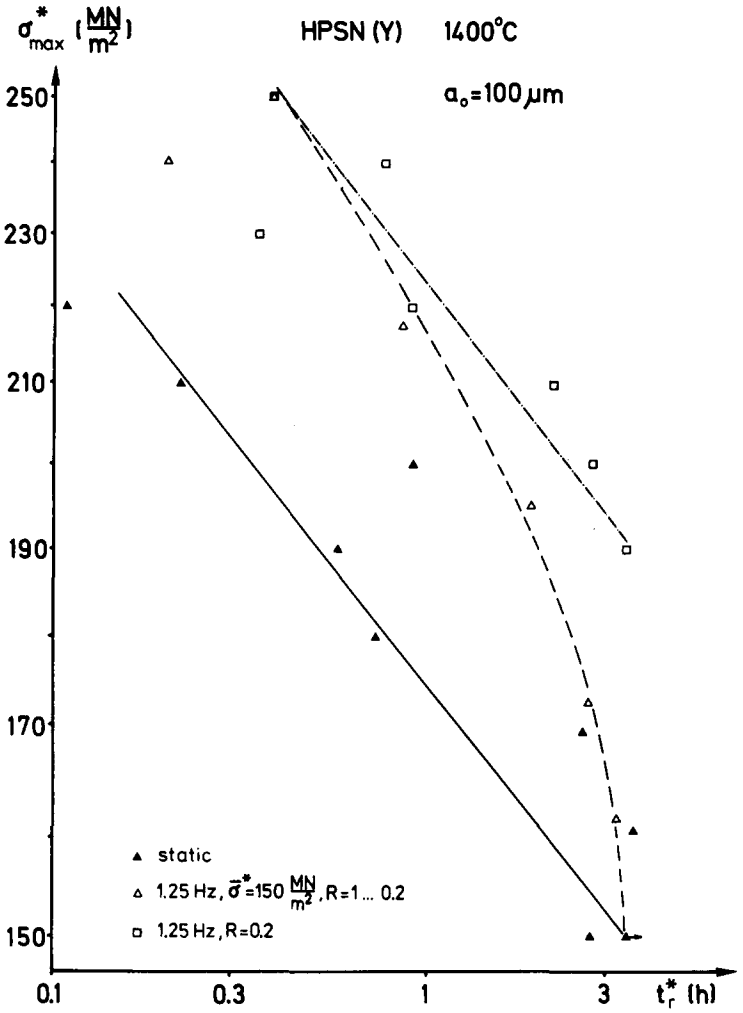

Fig. 22. HPSN(Y): time to failure under static and cyclic loading, dashed lines are calculated from static data ($R = \sigma^*_{min}/\sigma^*_{max}$).

A change of the rate controlling factor occurs, when passing from primary to secondary creep. Increasing grain linkage, or else increasing number of contact points between grains, decrease the creep rate. Stationary conditions are reached when the ratio of contact points, removed by diffusion, and added by creep deformation, is 1. The stress dependence of the nucleation of voids or microcracks and the growth of the hollow volume in accommodation to creep deformation, may lead to the different measured stress dependences, dependent on the kind of experiment considered (static, dynamic or strain controlled).

ACKNOWLEDGEMENTS

The author wishes to thank H. Iwanek for experimental assistance, G. Grathwohl and T. Fett for critical discussions.

REFERENCES

1. Lange, F. F., Silicon nitride polyphase systems: Fabrication microstructure and properties, Rev. 247, *Int. Met. Rev.* (1980) 1–20.
2. Grathwohl, G., Creep and fracture of hot-pressed silicon nitride with natural and artificial flaws, in *Creep and Fracture of Engineering Materials and Structures*, Eds B. Wilshire and D. R. J. Owen, Pineridge Press, Swansea, 1984, 515.
3. Cohrt, H., Grathwohl, G. and Thümmler, F., Instationary stress distribution in a ceramic bending beam during constant load creep, *Res Mechanica*, **10** (1984) 55.
4. Ernstberger, U., Oxidations—und Kriecherhalten von dichten Siliziumnitrid-werkstoffen verschiedener Zusammensetzung, Dr Thesis, University of Karlsruhe, 1985 (in German).
5. Schaeffer, H. A., Structure–property relationships of the vitreous state, in *Progress in Nitrogen Ceramics*, Martinus Nijhoff Publishers, Boston, 1983, 303–21.
6. Finnie, I., Method for predicting creep in tension and compression from bending tests, *J. Am. Ceram. Soc.*, **49** (1966), 218–20.
7. Talty, P. K. and Dirks, R. A., Determination of tensile and compressive creep behaviour of ceramic materials from bend tests, *J. Mat. Sci.*, **13** (1978) 580–6.
8. Kraus, H., Numerical analysis of creep, in *Creep Analysis*, John Wiley & Sons, New York, 1980.
9. Fett, T. and Munz, D., Determination of transient creep parameters for HPSN by dynamic bending tests, *J. Mat. Sci.*, **19** (1984) 1791–8.
10. Yen, T. S., Zhuang, H. R., Li, W. L., Wen, S. W. and Fu, X. R., Sintering characteristics of some fine Si_3N_4 powders by different preparatory methods, in *Proc. First International Symposium on Ceramic Components for Engine*, Eds S. Somiya, E. Kanai and K. Ando, D. Reidel Publ. Co., Dordrecht 1984, 218.
11. Lange, F. F., Non-elastic deformation of polycrystals with a liquid boundary phase, in *Deformation of Ceramic Materials*, Eds R. C. Bradt and R. E. Tressler, Plenum Press, New York, 1983, 341–81.
12. Griffith, A. A., The phenomena of rupture and flow in solids, *Phil. Trans. Roy. Soc. London*, **A221** (1921) 163–98.
13. Hasselman, D. P. H., Krohn, D. A., Bradt, R. C. and Coppola, T. A., The Griffith criterion and the reversible and irreversible fracture of brittle materials, in *Fracture Mechanics of Ceramics, Vol. 2*, Eds R. C. Bradt, D. P. H. Hasselman and F. F. Lange, Plenum Press, New York, 1974, 749–55.
14. Dutton, R., The propagation of cracks by diffusion, in *Fracture Mechanics of Ceramics, Vol. 2*, Eds R. C. Bradt, D. P. H. Hasselman and F. F. Lange, Plenum Press, New York, 1974, 647–57.

15. Brown, W. F. and Srawley, J. E. Plane strain crack toughness testing of high strength metallic materials, *ASTM STP 410*, Philadelphia, 1966.
16. Govila, R. K. Indentation-precracking and double-torsion methods for measuring fracture mechanics parameters in hot-pressed Si_3N_4, *J. Am. Ceram. Soc.*, **63** (1980) 319–26.
17. Evans, A. G. and Fuller, E. R., Crack propagation in ceramic materials under cyclic loading conditions, *Met. Trans.*, **5** (1974) 27–33.

Received 4 July 1986; revised version received 9 June 1987; accepted 20 June 1987